Discovery of selective diacylglycerol lipase β inhibitors

Zhu, N.

Chapter 7

Summary and Future Prospects

7.1 Summary

Endocannabinoids are the endogenous signaling lipids that activate cannabinoid receptors type 1 and 2 (CB_1R and CB_2R) to regulate various biological processes, such as synaptic plasticity, memory formation and learning, mood, energy metabolism, pain sensation and immune response.[1–4] There are two main endocannabinoids: 2-arachidonoylglycerol (2-AG)[5] and *N*-arachidonoylethanolamine (AEA, anandamide).[6] Endocannabinoids are produced 'on demand' by biosynthetic enzymes (*e.g.*, DAGLα/β[7] and NAPE-PLD[8]) and rapidly inactivated by metabolic enzymes (*e.g.*, MAGL[9] and FAAH[10]) to terminate their actions. Endocannabinoids, cannabinoid receptors CB_1R and CB_2R, biosynthetic and metabolic enzymes constitute the endocannabinoid system (ECS). To study biological functions and establish the therapeutic potential of these enzymes, a number of activity-based probes (ABPs) and small molecular inhibitors have been developed, as summarized in **Chapter 1**. Two types of broad-spectrum ABPs have been developed so far: fluorophosphonate-based probes[11,12] and β-lactone-based probes.[13,14] These probes can label numerous serine hydrolases, including most enzymes in the ECS, enabling novel inhibitor discovery and selectivity evaluation. Benefiting from the application of these probes in activity-based protein profiling (ABPP), many potent and selective inhibitors have been discovered for ECS enzymes. Representative inhibitors include, but are not limited to, DH376[15], a triazole urea-based dual DAGLα/β inhibitor; LEI-401[16], a pyrimidine-4-carboxamide-based NAPE-PLD inhibitor; Lu AG06466[17], a carbamate-based MAGL inhibitor; and PF-04457845[18], a pyridazine urea-based FAAH inhibitor.

Additionally, in **Chapter 1**, the biological functions and potential clinical applications of targeting ECS enzymes are discussed. MAGL and FAAH inhibitors have progressed to clinical trials. The MAGL inhibitor, Lu AG06466, demonstrated general safety in clinical trials but did not exhibit efficacy in reducing tics, premonitory urges and comorbidities in patients with Tourette syndrome during a phase 2 clinical trial.[19] The FAAH inhibitor PF-04457845 showed positive effects in a phase 2a study on cannabis use disorder.[20] Another FAAH inhibitor, JNJ-42165279, is currently under clinical investigation for treating post-traumatic stress disorder (PTSD). In contrast, the research progress of DAGL and NAPE-PLD inhibitors has been slower and they are currently being studied in animal models. DAGL inhibitors have showed anti-inflammatory[15,21] effects and analgesic effects.[22] However, inhibiting DAGLα in the brain might potentially lead to psychiatric side effects.[23,24] The first-in-class NAPE-PLD inhibitor, LEI-401, was found to activate the hypothalamus–pituitary–adrenal (HPA) axis and impair fear extinction in mice.[16] In this context, peripherally restricted inhibitors can be essential tools to elucidate the functions of ECS enzymes in peripheral tissues and may have new clinical applications. Moreover, potent and selective inhibitors are still lacking for some ECS enzymes, such as DAGLα and DAGLβ.

The development of selective DAGLβ inhibitors is crucial for understanding the distinct biological functions of this enzyme and discerning the roles of DAGLβ and DAGLα under specific pathophysiological conditions. Moreover, selective DAGLβ inhibitors hold a promise as a valuable approach for treating inflammatory diseases while minimizing the potential for

central nervous system (CNS)-mediated side effects. Therefore, the primary objective of the research outlined in this thesis is to advance the development of selective DAGLβ inhibitors.

In **Chapter 2**, a fluorescence assay using EnzChek lipase substrate was optimized for DAGLα/β and miniaturized to a 384-well plate format. This assay was subsequently applied in a high-throughput screening (HTS) using the purified catalytic domain of DAGLβ to identify new hit compounds. A library of 12,560 serine hydrolase inhibitors from Enamine and an in-house library of 27 glycine sulfonamides[25] were screened at 10 μM. After primary screening, confirmed screening, deselection, and dose-response determination, eight hits classified into four chemotypes were identified, including glycine sulfonamide (hit **1**), ketones (hits **2**, **5**), ureas (hits **3**, **4**) and cyano amides (hits **6-8**). Hit **1**, also known as LEI-106[25] (Figure 7.1A), exhibited the highest potency for DAGLβ with a pIC_{50} of 6.69 ± 0.14 and promising physicochemical properties, but was not selective over DAGLα (pIC_{50} of 7.35 ± 0.06).

In **Chapter 3**, a structure-activity relationship (SAR) study for both DAGLα and DAGLβ was conducted, starting from hit **1**, with the aim of enhancing the potency and selectivity specifically for DAGLβ. A total of 51 analogues were synthesized and biochemically evaluated, resulting in the identification of compound **9** as the most potent and selective DAGLβ inhibitor, albeit a modest selectivity of 2.7-fold (Figure 7.1A). The SAR study revealed that the sulfonyl group was a modification hotspot for improving selectivity, while other components contributed to potency to varying extents.

In **Chapter 4**, an extensive SAR study was conducted, with a specific focus on modifying the sulfonyl group to enhance DAGLβ selectivity. The introduction of a cyclobutyl substituent on the amine moiety and the modification of the dibenzo[*b*,*d*]furan on the sulfonyl group of compound **9** to a 2,3-dihydrobenzo[*b*][1,4]dioxine resulted in compound **10**, which exhibited improved potency (pIC_{50} of 7.59 ± 0.06) and selectivity (20-fold) for DAGLβ (Figure 7.1A). Expanding the dioxane ring in compound **10** to a dioxepane yielded compound **11** with further increased selectivity. However, other modifications on the sulfonyl resulted in less selective compounds. Changing the cyclobutyl in **11** to a cyclopentyl resulted in compound **12**, which displayed improved potency while retaining selectivity for DAGLβ. Replacing the bromide in compounds **11** and **12** with other electron-withdrawing and lipophilic moieties (*e.g.* chloride and trifluoromethyl) resulted in a series of compounds exhibiting high potency ($pIC_{50} > 7.50$), good selectivity (~40-fold), appropriate lipophilicity (cLogD < 3) and lipophilic efficiency (LipE > 5). The comprehensive SAR for glycine sulfonamide DAGL inhibitors is illustrated in Figure 7.1B.

In **Chapter 5**, a fluorescence-based 96-well plate assay was established to assess the cellular activity of DAGL inhibitors using Neuro2A cells expressing the $GRAB_{eCB2.0}$ sensor. This sensor is a circular permuted enhanced green fluorescent protein (cpEGFP)-modified CB_1 receptor[26] that can be activated by the binding of endocannabinoids to elicit fluorescence. The $GRAB_{eCB2.0}$ sensor expressed in Neuro2A cells responds to ATP-induced production of 2-AG. A total of 23 DAGL inhibitors were profiled in this assay, demonstrating a concentration-dependent reduction in the production of 2-AG with varying potencies. Significantly, a strong correlation was observed between the cellular activity in the Neuro2A $GRAB_{eCB2.0}$ assay and

the biochemical activity for DAGLα. However, no such correlation was identified for DAGLβ, indicating that DAGLα is the primary isoform involved in ATP-stimulated 2-AG production in Neuro2A cells.

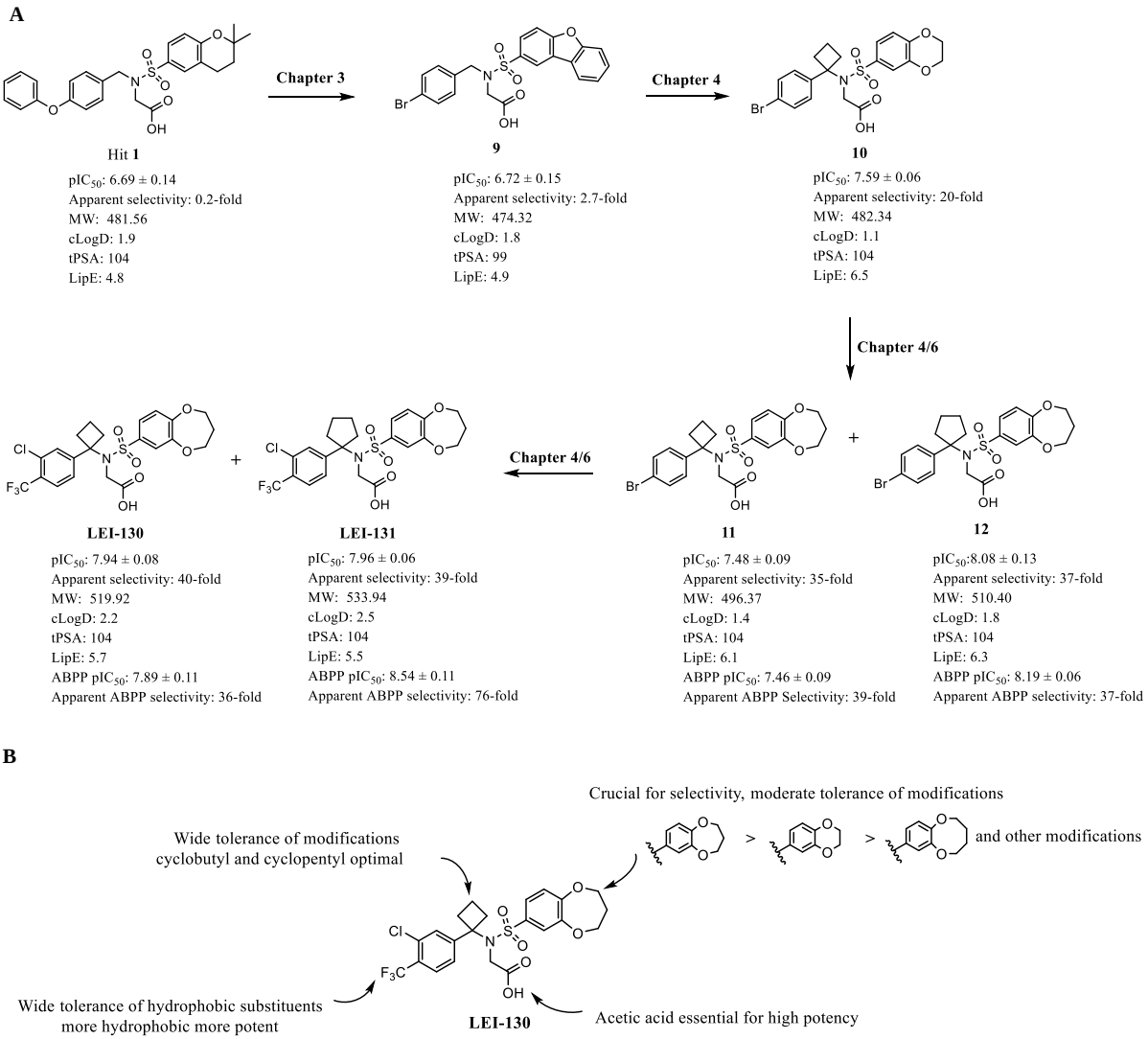

Figure 7.1 Summary of the structure-activity relationship (SAR) study. (A) Chemical structures, biochemical results (pIC_{50}, apparent selectivity and LipE for DAGLβ), physiochemical properties (MW, cLogD and tPSA) and activity-based protein profiling results (ABPP pIC_{50} and apparent ABPP selectivity for DAGLβ) of Hit **1** and representative compounds in SAR. (B) The overall SAR.

In **Chapter 6**, the most promising DAGLβ selective inhibitors developed in Chapter 4 underwent investigation in ABPP assays using DAGL-tailored probe DH379. Considering both potency and selectivity in biochemical and ABPP assays, along with structure similarities, **LEI-130** and **LEI-131** emerged as the most promising candidates for further *in vitro* and *in situ* profiling (Figure 7.1A). Michaelis-Menten kinetic studies using the EnzChek lipase substrate assay demonstrated that both LEI-130 and LEI-131 inhibited DAGLβ through a noncompetitive inhibition mode, suggesting their binding to an allosteric pocket of DAGLβ. *In vitro* selectivity profiling revealed that LEI-130 and LEI-131 did not affect the activity of NAPE-PLD, FAAH,

MAGL, ABHD6, ABHD12 and cannabinoid CB_1 and CB_2 receptors. *In situ* target engagement and selectivity profiling in microglia and macrophage cells confirmed cell permeability of LEI-130 and LEI-131, and their capability to inhibit endogenous DAGLβ without interfering with other serine hydrolases. Targeted lipidomics of LEI-130 and LEI-131 demonstrated an increase in SAG levels in N9 microglia cells and J774.1 macrophages. However, a decrease in the levels of 2-AG, arachidonic acid (AA), and prostaglandins PGE_2 and PGD_2 was only observed in N9 cells. LEI-132, a DAGL inactive compound included as a negative control, did not show any effects on 2-AG and SAG levels. This indicates that 2-AG production in J774.1 macrophages, unlike N9 microglia cells, is not dependent on DAGLβ. Interestingly, LEI-130, LEI-131 and LEI-132 were all shown to attenuate LPS-stimulated cytokine production, suggesting that an unknown off-target modulates LPS-stimulated cytokine production.

7.2 Future prospects

7.2.1 Photoaffinity labeling to identify the allosteric binding pocket

LEI-130 and LEI-131 were identified as allosteric inhibitors of DAGLβ utilizing a noncompetitive inhibition mechanism. To unveil the binding pocket of these compounds, an affinity-based photoprobe (**13**) was designed, incorporating a glycine sulfonamide pharmacophore, a diazirine for UV-activated protein crosslinking, and an alkyne handle for reporter ligation. The synthesis of the probe is depicted in Scheme 7.1. Weinreb amide **14** obtained from 4-pentanoic acid was transformed into ketone **15** via Grignard reaction. Subsequently, reductive amination of **15** with ethyl glycinate yielded amine **16**, followed by condensation with 2,2-dimethylchromane-6-sulfonyl chloride, resulting in sulfonamide **17**. THP deprotection afforded key intermediate **18**. Diazirine-linker **20** was obtained from 4-hydroxybutan-2-one by diaziridine introduction under agency of NH_3 and NH_2OSO_3H, followed by oxidation with I_2 to form compound **19**. The hydroxyl group was then transformed to a toysl-ester leaving group (**19** → **20**). Alkyation of **18** with **20** afforded ether **21**, which, after saponification, resulted in the final photoprobe **13**.

The inhibitory activity of photoprobe **13** for DAGL enzymes was assessed in the EnzChek lipase substrate assay, resulting in similar pIC_{50} values for DAGLα and DAGLβ (Figure 7.2).

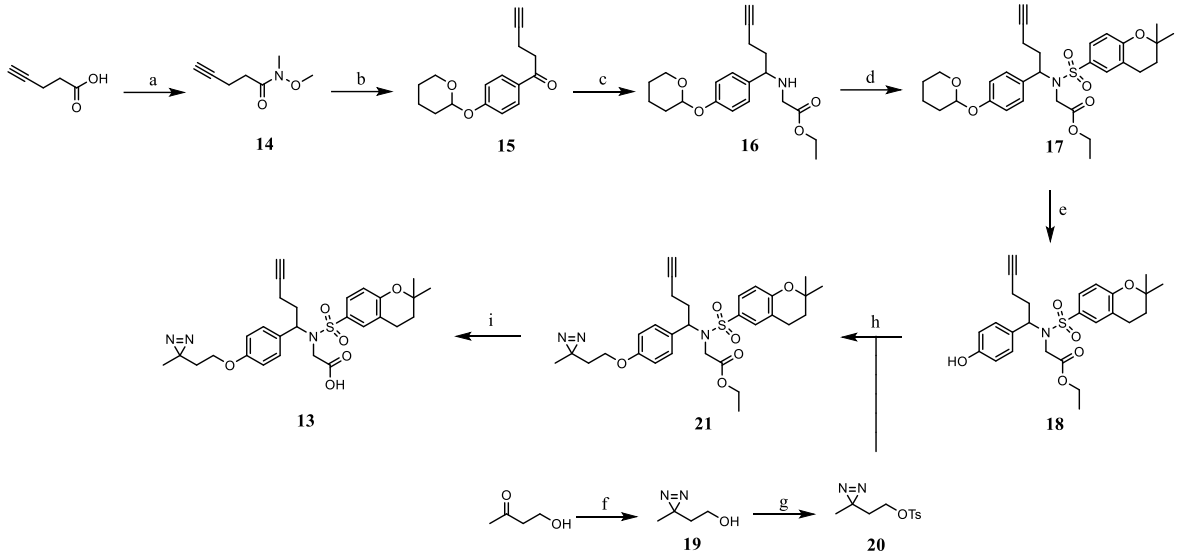

Scheme 7.1 Synthesis of photoprobe **13**. a) *N*,*O*-dimethylhydroxylammonium chloride, DMAP, EDCI, Et_3N, anhydrous DCM, rt, 42%; b) (4-((tetrahydro-2*H*-pyran-2-yl)oxy)phenyl)magnesium bromide, anhydrous THF, 0 °C-rt, 41%; c) glycine ethyl ester hydrochloride, Et_3N, AcOH, $NaBH_3CN$, anhydrous EtOH, reflux, 49%; d) 2,2-dimethylchromane-6-sulfonyl chloride, DMAP, Et_3N, anhydrous DCM, rt, 75%; e) TsOH, EtOH, rt, 70%; f) *i*. 7 N NH_3 in MeOH, 0 °C; *ii*. NH_2OSO_3H, anhydrous MeOH, rt; *iii*. Et_3N, I_2, anhydrous MeOH, 21%; g) 4-methylbenzenesulfonyl chloride, pyridine, rt, 57%; h) Cs_2CO_3, anhydrous DMF, rt, 25%; i) 1 M aq. LiOH, THF/MeOH, rt, 29%.

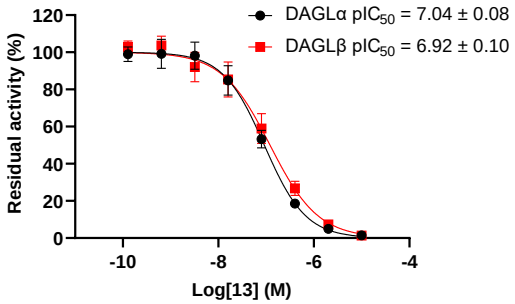

Figure 7.2. Dose-response curves of photoprobe **13** for DAGLα (black) and DAGLβ (red). Data shown are mean ± SD (n = 1, N = 3).

Next, it was tested whether probe **13** could label recombinant human DAGL in HEK293T lysates in a specific manner. DMSO or DAGL inhibitors (DO34, KT109, LEI-105 and LEI-106, Figure 7.3B) were incubated for 30 min before adding probe **13** (100 nM). The mixture was incubated for 10 min, irradiated with 350 nm UV light for 10 min and clicked with a Cy5-N_3 fluorophore (1 μM) for 45 min. The click reaction was quenched by adding Laemmli blue and resolved by sodium dodecyl sulfate polyacrylamide gel electrophoresis (SDS-PAGE). Strong fluorescent bands at the expected molecular weights of ~120 kDa and ~70 kDa appeared in the HEK293T cell lysates overexpressing DAGLα and DAGLβ, respectively (lane 2 and 7, Figure 7.3A), but not in the mock lysate (lane 1, Figure 7.3A). Pre-incubation with DAGL inhibitors DO34, KT109 at 1 μM, and LEI-105 and LEI-106 at 10 μM reduced the labeling of these bands. This indicated the successful engagement of DAGLα and DAGLβ by probe **13** and the inhibitors. The activity of DAGLβ selective inhibitors, LEI-130 and LEI-131, was assessed

using photoprobe **13**. The results demonstrated that both LEI-130 and LEI-131 effectively inhibited the labeling of DAGLβ by probe **13** in a concentration-dependent manner (Figure 7.4A), exhibiting pIC_{50} values of 7.12 ± 0.13 and 7.59 ± 0.22 (Figure 7.4B), respectively.

To identify the photoprobe-labeled DAGLβ peptides, chemical proteomics was conducted. However, MS-based proteomics did not enable the identification of these peptides, thereby impeding the elucidation of the allosteric binding pocket of glycine sulfonmaides on DAGLβ.

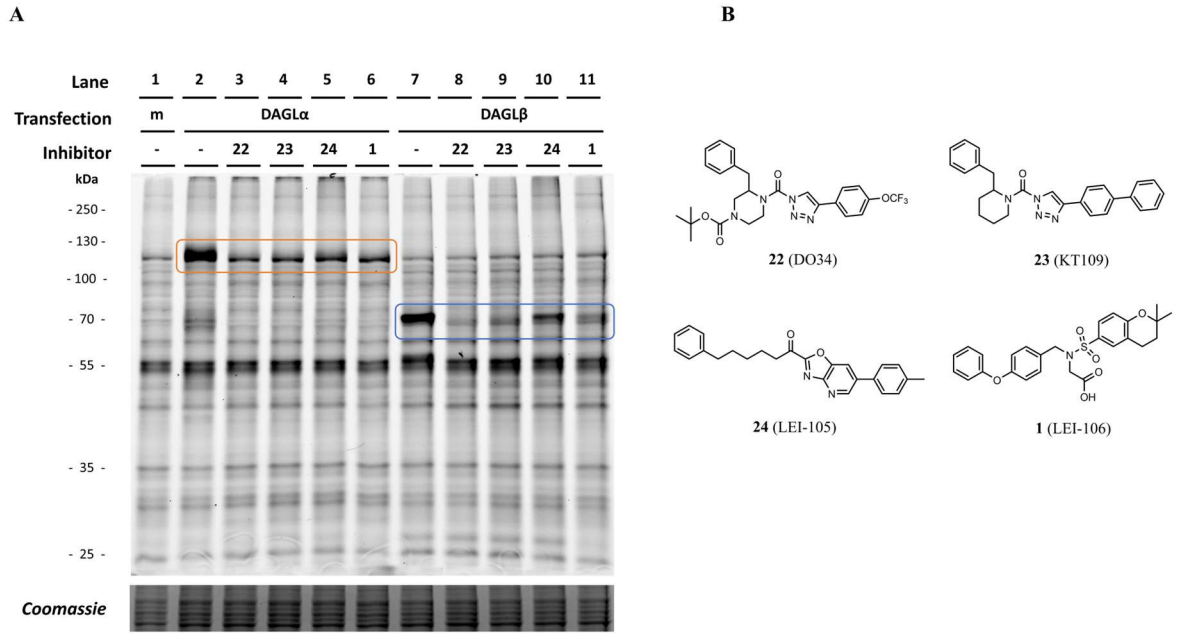

Figure 7.3 Photoprobe **13** enabled *in vitro* labeling and visualization of recombinant human DAGLα and DAGLβ. (A) Representative gel of fluorescent labeling of DAGLα (orange) and DAGLβ (blue) by photoprobe **13** without or with DAGL inhibitors. (B) Chemical structures of DAGL inhibitors DO34, KT109, LEI-105 and LEI-106.

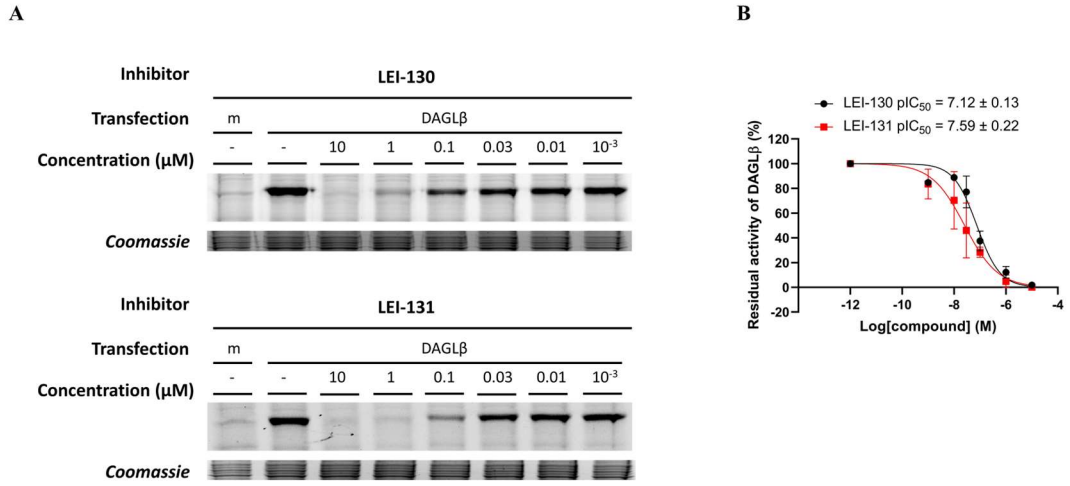

Figure 7.4 LEI-130 and LEI-131 concentration-dependently blocked the labeling of DAGLβ by probe **13**. (A) Representative gel excerpts of fluorescent labeling of DAGLβ by probe **13** without or with LEI-130 and LEI-131 at different concentrations. (B) Dose-response curves of LEI-130 and LEI-131 for DAGLβ. Data shown are mean ± SD (n = 1, N = 3).

7.2.2 Ethyl ester protection is not an effective prodrug strategy for glycine sulfonamide DAGL inhibitors.

In Chapter 5, a set of glycine sulfonamide DAGL inhibitors was assessed in the Neuro2A $GRAB_{eCB2.0}$ assay, revealing a significant decrease in their cellular activity compared to their biochemical activity. The reduction in activity is likely primarily due to the low cell permeability of glycine sulfonamides caused by the carboxylic acid. To enhance cell permeability and cellular activity, the carboxylic acid of LEI-130 and LEI-131 was protected by an ethyl ester in a prodrug approach, resulting in compounds **25** and **26** (Figure 7.5A). When evaluated in the EnzChek lipase substrate assay, compounds **25** and **26** displayed no activity for either DAGLα or DAGLβ (pIC_{50} < 5, Figure 7.5B, C).

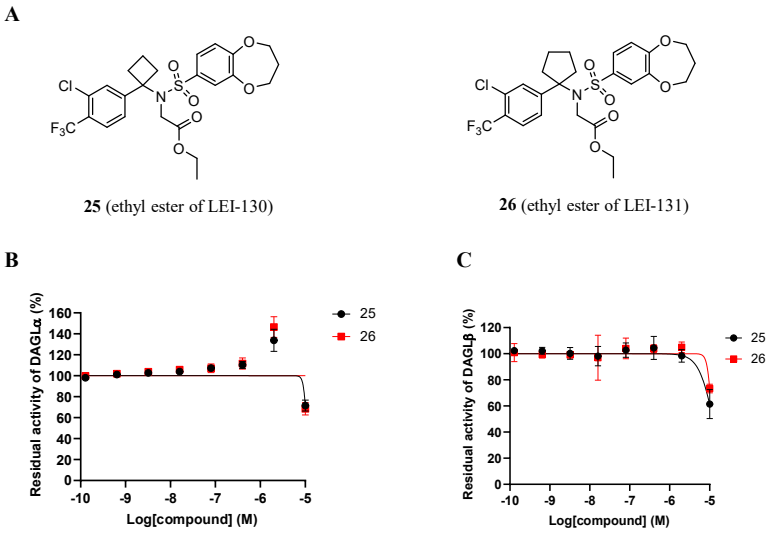

Figure 7.5 Compounds **25** and **26** were not active for DAGL enzymes. (A) Chemical structures of compounds **25** and **26**. (B, C) Dose-response curves of compounds **25** and **26** for DAGLα (B) and DAGLβ (C). Data shown are mean ± SD (n = 1, N = 3).

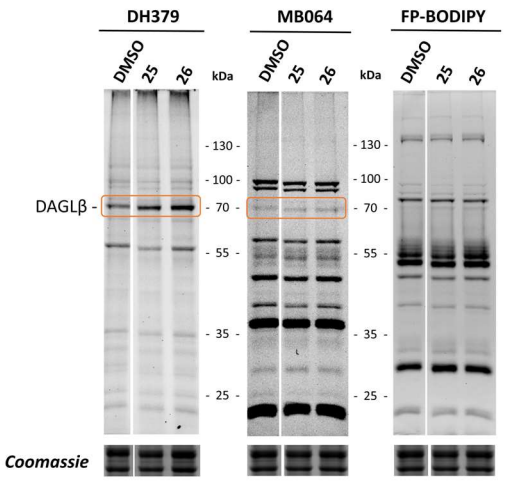

Figure 7.6 *In situ* target engagement and selectivity of compounds **25** and **26**. Representative gels of ABPP experiments with compounds **25** and **26** (10 µM, 2 h) in N9 microglia using DH379 (*in situ*, 1 µM, 1 h) or the cocktail of MB064 and FP-BODIPY (*in vitro*, 100 nM, 10 min).

To investigate whether compounds **25** and **26** could undergo hydrolysis to form active DAGLβ inhibitors in cells, *in situ* gel-based ABPP was conducted in N9 microglia cells, as described in Chapter 6. However, compounds **25** and **26** were not converted to the active parents LEI-130 and LEI-131, as endogenous DAGLβ was not inhibited. Therefore, protecting the carboxyl group with an ethyl ester is not an effective prodrug strategy for glycine sulfonamide DAGL inhibitors.

7.2.3 Targeting DAGLβ-DAG-PKC axis to regulate antitumor immunity

Diacylglycerol (DAG) functions as a physiological activator of protein kinase C (PKC), orchestrating cellular processes.[27] The production of DAG in the plasma membrane from phosphatidylinositol 4,5-bisphosphate (PIP_2) is mediated by phospholipase C (PLC). Subsequently, DAG is metabolized by DAGL and diacylglycerol kinase (DGK) to form monoacylglycerol (MAG) and phosphatidic acid (PA), respectively. DAG interacts with the C1 domain of its effector proteins such as PKC, leading to their recruitment to the membrane.[28,29] The membrane interaction induces a conformational change of PKC, representing a pivotal step to activate PKC. Activated PKC catalyzes the phosphorylation of hydroxyl groups on serine and threonine amino acid residues of its substrates, initiating downstream signaling activation.[27,30] The delicate balance in the biosynthesis and degradation of DAG, as well as the precise regulation of PKC, is crucial for cellular homeostasis. PKC isoenzymes demonstrate a dual role in cancer, acting as both promoters and suppressors, with their specific functions intricately tied to the isoform and cellular context. A distorted pattern of PKC isoenzyme expression has been discovered in most cancer cells, including up-regulation of PKCε, PKCη and PKCθ with oncogenic activities[31–37] and down-regulation of PKCα, PKCβ and PKCδ with tumor-suppressing functions.[38–43] This underscores the complexity of PKC isoenzymes across various cancer types.

Tumor progression is regulated by the interaction between cancer cells and tumor microenvironment (TME).[44] DAG and its effectors exert their influence not only on cancer cells but also extend to noncancerous cells within the TME. DAG plays a pivotal role as a messenger lipid in T cell activation via the T cell receptor (TCR) and tightly regulates the dynamic relationship between cancer cells and T cells.[27,45,46] Within T cells, DAG interacts with the C1 domain to recruit DAG effectors to the immunological synapse. The translocation of DAG effectors triggers the activation of essential transcriptional machinery that governs T cell expansion and activity. PKC signals stimulate the production of interleukin-2 (IL-2), a key cytokine for T cell proliferation and differentiation, as well as tumor necrosis factor-α (TNF-α) and interferon-γ (IFN-γ), cytokines contributing to the inhibition of cancer cells.[47] Recently, the production of DAG during T cell receptor signaling was shown to trigger ectocytosis of activated TCRs.[48] The resulting budding ectosomes could be directly endocytosed by target cells, leading to the termination of TCR signaling. Concurrently, the process separates cytotoxic T lymphocytes (CTLs) from target cells, thereby facilitating serial killing. Therefore, maintaining sufficient DAG levels is important for T cell activity and function.

Down-regulated DAG response observed in tumor-infiltrating lymphocytes (TILs) is a hallmark, contributing to hyporesponsive state and reduced lytic activity.[49] Small molecules capable of restoring DAG response could serve as potential treatments to enhance the antitumor potential of cytotoxic T lymphocytes. Diacylglycerol lipase β (DAGLβ) is the predominant enzyme responsible for hydrolyzing DAG in primary macrophage[21] and dendritic cells.[50] DAGLβ disruption in dendritic cells has been discovered to reduce the production of inflammatory cytokine without affecting their capacity for $CD8^+$ T cell priming.[50] However, the involvement of DAGLβ in cancer and antitumor immunity remains understudied. In this research, selective DAGLβ inhibitors, LEI-130 and LEI-131, have been successfully developed. Lipidomics studies demonstrated their ability to significantly elevate the levels of stearoyl-arachidonoyl DAG (SAG) in N9 microglia and J774A.1 macrophages. LEI-130 and LEI-131 hold potential as valuable tool compounds for unraveling the intricate role of DAGLβ in both cancer cells and T cells, with promising applications in cancer therapy.

7.3 Closing remarks

Selective and cellularly active small molecules play a pivotal role in elucidating the physiological and pathological functions of enzymes, as well as in the development of novel therapies. The research described in this thesis presents a reliable biochemical assay for DAGLα and DAGLβ, applicable for high-throughput screening of DAGLβ inhibitors. These methods are anticipated to streamline future drug discovery studies targeting DAGL. Notably, this research details the development of LEI-130 and LEI-131 as pioneering DAGLβ-selective and cellularly active inhibitors, functioning through a noncompetitive inhibition mode. As first-in-class selective DAGLβ inhibitors, LEI-130 and LEI-131 serve as valuable chemical tools to advance our understanding of DAGLβ and unveil its therapeutic potentials.

7.4 Acknowledgements

Matthijs R. van Wijngaarden is acknowledged for evaluating the activity of LEI-130 and LEI-131 in affinity-based protein profiling using the photoprobe. Dr. Stephan M. Hacker is kindly acknowledged for measuring proteomics samples and data analysis. Hans van den Elst is kindly acknowledged for HRMS measurements.

7.5 Experimental methods

Biology

EnzChek lipase substrate assay for DAGLα and DAGLβ in 384-well plate

The DAGL EnzChek lipase substrate assay was performed as described in Chapter 3.

Gel-based photoaffinity labeling

19 µL of HEK293T cell lysate overexpressing DAGLα or DAGLβ was incubated with either 0.5 µL DMSO or inhibitors (40× concentrated stocks in DMSO) for 30 min. As a negative control, mock lysate incubated with DMSO was used. 0.5 µL of the photoprobe (40× concentrated stocks in DMSO, final concentration 100 nM) was added and incubated for 15 min before irradiation under UV (Caprobox, 350 nm) for 10 min at 4 °C. Subsequently, 2.22 µL of click mix (final concentrations: 1 mM $CuSO_4$, 6 mM sodium ascorbate, 1 mM THPTA, and 1 µM Cy5-N_3) was added and incubated for 45 min in the dark. 7.4 µL of Laemmli blue (4×) was added and incubated for 10 min to quench the reaction. 10 µL of the quenched reaction mixture was resolved by 10% SDS-PAGE (180 V, 80 min) and the fluorescence was measured in a Biorad ChemiDoc™ MP system (Cy5: 700/50 filter; Cy3: 602/50 filter). The remaining activity was determined by measuring the integrated fluorescence using Image Lab™ 6.0.0, which was corrected for the total protein loading per lane as determined by Coomassie stain (R250) and imaging (Coomassie Blue Gel: 590/110 filter). The IC_{50} values were determined from a dose-response curve generated using GraphPad Prism 9.0.0 software (log(inhibitor) vs. normalized response with variable slope). The assay was performed three times independently (n = 1, N=3).

MS-based proteomics

1 mL of HEK293T cell lysate overexpressing DAGLβ or mock was incubated with 26 µL of the photoprobe (40× concentrated stocks in DMSO, final concentration 100 nM) for 30 min before irradiated under UV (Caprobox, 350 nm) for 10 min at 4 °C. 114 µL of click mix (final concentrations: 1 mM CuSO4, 6 mM sodium ascorbate, 1 mM THPTA, and 1 µM desthiobiotin-N_3) was added and incubated for 1 h in the dark. The proteins were precipitated in 4 mL cold acetone at -20 °C for overnight. Samples were centrifuged for 10 min at 3,500 g and the supernatants were carefully aspirated. The remaining proteins were washed twice with 1 mL of -80 °C methanol by resuspending using sonication (20% amplitude, 10 s), centrifugation (3,500 g, 3 min), and removing the supernatant. For trypsin digestion, the precipitated proteins were suspended in 300 µL urea buffer (8 M urea in 0.1 M TEAB) by sonication (80% amplitude, 20 s). The samples were spun down (1000 rpm, 1 min) before adding 15 µL of 31 mg/mL DTT and incubation at 37 °C for 45 min with shaking (500 rpm). After this, 15 µL of 74 mg/mL iodoacetamide was added and incubated in the dark for 30 min with rotating. 900 µL of 0.1 M TEAB was added to dilute the sample and 10 µL of 2 mg/mL trypsin was added and incubated at 37 °C for overnight in a shaking incubator (500 rpm). For chymotrypsin digestion, the

precipitated proteins were suspended in 300 µL urea buffer (8 M urea in 0.1 M Tris-HCl at pH 8.0) by sonication (80% amplitude, 20 s). The samples were spun down (1000 rpm, 1 min) before adding 15 µL of 31 mg/mL DTT and incubation at 37 °C for 45 min with shaking (500 rpm). After this, 15 µL of 74 mg/mL iodoacetamide was added and incubated in the dark for 30 min with rotating. 2.1 mL of 0.1 M Tris-HCl at pH 8.0 with 11.43 mM $CaCl_2$ was added to dilute the sample and 20 µL of 1 mg/mL chymotrypsin was added and incubated at 25 °C for overnight in a shaking incubator (500 rpm). 50 µL of Streptavidin high-capacity beads (Thermo Scientific) was added to Falcon tubes and washed three times with PBS by resuspending, centrifugation (1,000 g, 3 min), and removing the supernatant. The washed beads were then suspended in 1.2 mL PBS before adding the digested sample. The mixture of beads and peptides were incubated for 1 h while rotating. The samples were spun down (1,000 g, 3 min) and the supernatants were removed. The remaining beads were suspended in 600 µL PBS and transferred to a Biospin column. The solution was aspirated and the beads were washed twice with 600 µL PBS, three times with 600 µL H_2O, and three time with 600 µL 50% ACN. The columns with beads were then transferred to a 1.5 mL Low-bind Eppendorf tube and the peptides were eluted from the beads using 200 µL of 50% ACN with 0.1% TFA. The elution step was repeated twice using 70 µL of 50% ACN with 0.1% TFA and completed by centrifugation (3,000 g, 3 min). The samples were evaporated at 45 °C to dryness using SpeedVac. The remaining peptides were dissolved in 30 µL of 0.1% TFA in water by pipetting up and down, sonicating (20% amplitude, 10 s), and centrifugation (2,000 g, 1.5 min). Finally, the peptide solutions were filtered through a pre-washed filter (UFC30GVNB) and transferred to MS sample vials.

Fractionated peptide samples were analyzed using a nanoElute 2 LC system (Bruker) coupled to a timsTOF HT mass spectrometer (Bruker). 5 µL of sample was loaded on a trap column (PepMap C18, 5 mm × 0.3 mm, 5 µm, 100 Å, Thermo Scientific) followed by elution and separation on the analytical column (PepSep C18, 25 cm × 75 µm, 1.5 µm, 100 Å, Bruker). A gradient of 2-25% solvent B (0.1% FA in ACN) in 25 min, 25-32% B in 5 min, 32-95% in 5 min and 95% B for 10 min at a flow rate of 300 nL/min (all% values are v/v, water, TFA and ACN solvents were purchased from Bisolve, LC-MS grade). ZDV Sprayer 20 µm (Bruker) installed in the nano-electrospray source (CaptiveSpray source, Bruker) was used with following source parameters: 1600 V of capillary voltage, 3.0 L/min of dry gas, and 180 °C of dry temperature. The MS data was acquired in DDA PASEF mode with an ion mobility window of 0.85 to 1.35 Vs/cm^2 in a mass range from 100 m/z to 1700 m/z with charge states from 0 to 5^+. The dual TIMS analyzer was utilized under a fixed duty cycle, incorporating a 100 ms ramp time, resulting in a total cycle time of 1.17 s. Precursors that reached a target intensity of 20,000 (intensity threshold 2,500) were selected for fragmentation and dynamically excluded for 0.4 min (exclusion window: mass width 0.015 m/z; 1/K0 width 0.015 Vs/cm^2). The collision energy was set to 20 eV at 0.6 Vs/cm^2 and 59 eV at 1.6 Vs/cm^2. The 1/K0 values in between were interpolated linearly and kept constant above or below. The quadrupole isolation width was set to 2 m/z for 700 m/z and to 3 m/z for 800 m/z. Isolation width was constant except for linear interpolation between specified points. For calibration of the TIMS elution voltage, the Agilent

ESI-Low Tuning Mix was used with three selected ions (m/z, 1/K0: 622.0290, 0.9915; 922.0098, 1.1986; 1221.9906, 1.3934). Mass calibration is performed with Na Formate in HPC mode.

In situ target engagement and selectivity in N9 microglia

In situ target engagement and selectivity profiling was performed as described in Chapter 6.

Chemistry

General remarks

All purchased chemicals were used without purification unless stated otherwise. All reactions were performed in oven-dried or flame-dried glassware. Anhydrous solvents were dried by activated 3 Å or 4 Å molecular sieves. Traces of water in starting materials were removed by co-evaporation with toluene if necessary. Thin layer chromatography (TLC) analysis was performed on Merck silica gel 60 F_{254} aluminium sheets and the compounds were visualized by using UV absorption at 254 nm and/or $KMnO_4$ staining (5 g/L $KMnO_4$ and 25 g/L K_2CO_3 in water). TLC plates were analysed with the Advion CMS Plate Express® connected to the Advion Expression® L-MS using 90% MeOH in H_2O with 0.1% formic acid as the solvent. Liquid chromatography-mass spectrometry (LC-MS) analysis was performed on a Thermo Finnigan LCQ Advantage MAX ion-trap mass spectrometer (ESI^+) coupled to a Surveyor HPLC system equipped with a C18 column (50×4.6 mm, 3 μm particle size, Macherey-Nagel) or a Thermo Finnigan LCQ Fleet ion-trap mass spectrometer (ESI^+) coupled to a Vanquish UHPLC system using H_2O, CH_3CN and 0.1% aq. TFA as eluents. Purification was performed on manual silica gel column chromatography (40-63 μm, 60 Å silica gel, Macherey-Nagel) or automated silica gel column chromatography (40-63 μm, 60 Å pre-packed silica gel, Screening Devices) on a Biotage Isolera™ Four 3.0 system. ^1H and ^{13}C spectra were recorded on a Bruker AV 400 MHz (400 MHz for ^1H and 101 MHz for ^{13}C) or AV 500 MHz spectrometer (500 MHz for ^1H and 126 MHz for ^{13}C) in deuterated solvents. Chemical shifts are reported in ppm with tetramethylsilane (TMS) or solvent resonance as the internal standard ($CDCl_3$: δ 7.26 for ^1H, δ 77.16 for ^{13}C). Data is reported as follows: chemical shifts δ (ppm), multiplicity (s = singlet, d = doublet, dd = doublet of doublets, ddd = doublet of doublet of doublets, dt = doublet of triplets, t = triplet, td = triplet of doublets, tt = triplet of triplets, q = quartet, quintet = p, bs = broad singlet, m = multiplet), coupling constants *J* (Hz) and integration. High resolution mass spectrometry (HRMS) analysis was performed on a Thermo Finnigin LTQ Orbitrap mass spectrometer equipped with an electrospray ion source in positive mode (source voltage 3.5 kV, sheath gas flow 10 mL/min, capillary temperature 250 °C) with resolution R = 60000 at m/z 400 (mass range m/z = 150-2000) and dioctyl phthalate (m/z = 391.28428) as a lock mass.

_N_-((2,2-Dimethylchroman-6-yl)sulfonyl)-_N_-(1-(4-(2-(3-methyl-3_H_-diazirin-3-yl)ethoxy)phenyl)pent-4-yn-1-yl)glycine (13)

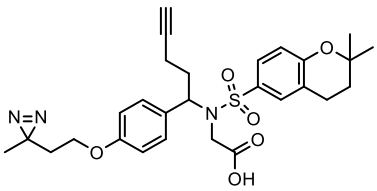

To a solution of ethyl _N_-((2,2-dimethylchroman-6-yl)sulfonyl)-_N_-(1-(4-(2-(3-methyl-3_H_-diazirin-3-yl)ethoxy)phenyl)pent-4-yn-1-yl)glycinate (**21**, 7.3 mg, 0.013 mmol, 1 eq) in THF/MeOH (280 µL/280 µL, 0.02 M) was added 1 M aq. LiOH (77 µL, 0.077 mmol, 6 eq). The mixture was stirred at rt for 20 h. The reaction mixture was diluted in EtOAc and washed with 0.2 M aq. HCl and brine. The organic layer was dried over anhydrous Na_2SO_4, filtered and concentrated. The residue was purified by silica gel column chromatography (0-5% MeOH in DCM) to obtain the impure product, which was purified again by silica gel column chromatography (10-30% EtOAc in _n_-pentane with a drop of conc. HCl) to obtain the pure product (2.0 mg, 3.7 µmol, 29%). ^{1}H NMR (500 MHz, $CDCl_3$) δ 7.62 – 7.58 (m, 2H), 7.08 – 7.03 (m, 2H), 6.87 – 6.83 (m, 1H), 6.81 – 6.76 (m, 2H), 5.06 (t, _J_ = 7.4 Hz, 1H), 3.94 (d, _J_ = 18.3 Hz, 1H), 3.83 (t, _J_ = 6.3 Hz, 2H), 3.68 (d, _J_ = 18.3 Hz, 1H), 2.79 (t, _J_ = 6.7 Hz, 2H), 2.20 – 2.08 (m, 3H), 2.06 – 1.99 (m, 1H), 1.97 (t, _J_ = 2.5 Hz, 1H), 1.85 (t, _J_ = 6.7 Hz, 2H), 1.81 (t, _J_ = 6.2 Hz, 2H), 1.37 (s, 6H), 1.11 (s, 3H). ^{13}C NMR (126 MHz, $CDCl_3$) δ 172.68, 158.66, 158.44, 130.04, 130.03, 129.65, 129.00, 127.51, 121.68, 118.08, 114.81, 83.18, 75.97, 69.36, 63.05, 59.43, 44.90, 34.39, 32.38, 30.68, 26.96, 24.39, 22.48, 20.39, 15.95. HRMS $[C_{28}H_{33}N_3O_6S+Na]^+$: 562.19823 calculated, 562.19824 found.

_N_-Methoxy-_N_-methylpent-4-ynamide (14)

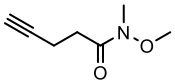

To a solution of 4-pentynoic acid (1.00 g, 10.2 mmol, 1 eq) in anhydrous DCM (25 mL, 0.4 M) was added DMAP (125 mg, 1.02 mmol, 0.1 eq), EDCI (4.00 g, 20.9 mmol, 2.05 eq), Et_3N (1.56 mL, 11.2 mmol, 1.1 eq) and _N_,_O_-dimethylhydroxylammonium chloride (1.09 g, 11.2 mmol, 1.1 eq). The mixture was stirred at rt for overnight. The reaction mixture was filtered through Celite and the filtrate was concentrated. The residue was purified by silica gel column chromatography (10-30% EtOAc in _n_-pentane) to afford the product (600 mg, 4.25 mmol, 42%). ^{1}H NMR (400 MHz, $CDCl_3$) δ 3.71 (s, 3H), 3.19 (s, 3H), 2.74 – 2.65 (m, 2H), 2.55 – 2.49 (m, 2H), 2.00 (t, _J_ = 2.6 Hz, 1H). ^{13}C NMR (101 MHz, $CDCl_3$) δ 172.27, 83.37, 68.65, 61.23, 32.09, 31.03, 13.76.

1-(4-((Tetrahydro-2_H_-pyran-2-yl)oxy)phenyl)pent-4-yn-1-one (15)

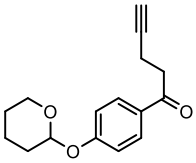

To a solution of _N_-methoxy-_N_-methylpent-4-ynamide (**14**, 166 mg, 1.18 mmol, 1 eq) in anhydrous THF (6 mL, 0.18 M) at 0 °C under argon was slowly added (4-((tetrahydro-2_H_-pyran-2-yl)oxy)phenyl)magnesium bromide (0.5 M in THF, 2.82 mL, 1.41 mmol, 1.2 eq). The resulting mixture was stirred at 0 °C for 3 h and rt for 3 h. A saturated aq. NH_4Cl solution (6 mL) was added to quench the reaction and the reaction mixture was extracted 3× with DCM. The combined organic layers were washed with brine, dried over anhydrous Na_2SO_4, filtered and concentrated. The residue was purified by silica gel column chromatography (2-4% EtOAc in _n_-pentane) to afford the

product as a white solid (124 mg, 0.480 mmol, 41%). ^{1}H NMR (400 MHz, $CDCl_3$) δ 7.96 – 7.90 (m, 2H), 7.12 – 7.05 (m, 2H), 5.51 (t, *J* = 3.1 Hz, 1H), 3.84 (ddd, *J* = 11.4, 9.9, 3.1 Hz, 1H), 3.66 – 3.58 (m, 1H), 3.22 – 3.15 (m, 2H), 2.64 – 2.57 (m, 2H), 2.06 – 1.93 (m, 2H), 1.91 – 1.83 (m, 2H), 1.77 – 1.55 (m, 3H). ^{13}C NMR (101 MHz, $CDCl_3$) δ 196.31, 161.15, 130.14, 116.02, 96.02, 83.57, 68.76, 62.02, 37.20, 30.08, 25.06, 18.48, 13.33.

Ethyl (1-(4-((tetrahydro-2*H*-pyran-2-yl)oxy)phenyl)pent-4-yn-1-yl)glycinate (16)

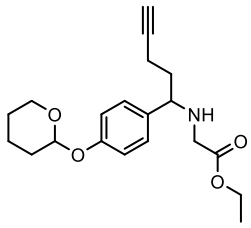

To a stirred solution of 1-(4-((tetrahydro-2*H*-pyran-2-yl)oxy)phenyl)pent-4-yn-1-one (**15**, 440 mg, 1.70 mmol, 1 eq) in anhydrous EtOH (15 mL, 0.12 M) with 4 Å molecular sieves was added glycine ethyl ester hydrochloride (713 mg, 5.11 mmol, 3 eq), Et_3N (710 µL, 5.11 mmol, 3 eq), AcOH (150 µL, 2.56 mmol, 1.5 eq) and $NaBH_3CN$ (118 mg, 1.87 mmol, 1.1 eq) at rt. The mixture was refluxed for overnight. The reaction mixture was filtered through Celite and the filtrate was concentrated. The residue was dissolved in EtOAc and washed 1× with sat. $NaHCO_3$ and brine, dried over anhydrous Na_2SO_4, filtered and concentrated. The residue was purified by silica gel column chromatography (10-15% EtOAc in *n*-pentane) to afford the product as a yellow oil (290 mg, 0.840 mmol, 49%). ^{1}H NMR (400 MHz, $CDCl_3$) δ 7.24 – 7.13 (m, 2H), 7.06 – 6.97 (m, 2H), 5.40 (t, *J* = 3.5 Hz, 1H), 4.14 (q, *J* = 7.1 Hz, 2H), 3.92 (ddd, *J* = 11.8, 9.3, 3.1 Hz, 1H), 3.71 (dd, *J* = 8.0, 5.4 Hz, 1H), 3.66 – 3.55 (m, 1H), 3.31 – 3.13 (m, 2H), 2.22 – 1.56 (m, 12H), 1.24 (t, *J* = 7.2 Hz, 3H). ^{13}C NMR (101 MHz, $CDCl_3$) δ 172.57, 156.56, 134.95, 128.47, 116.51, 96.49, 96.42, 83.99, 68.83, 62.23, 61.16, 61.09, 60.82, 48.76, 36.46, 30.48, 25.29, 18.94, 15.51, 14.26. LC-MS $[C_{20}H_{27}NO_4+H]^+$: 346.21 calculated, 345.73 found.

Ethyl *N*-((2,2-dimethylchroman-6-yl)sulfonyl)-*N*-(1-(4-((tetrahydro-2*H*-pyran-2-yl)oxy)phenyl)pent-4-yn-1-yl)glycinate (17)

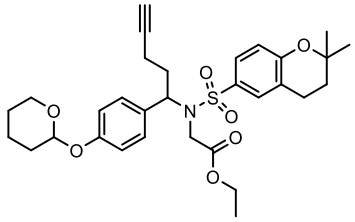

To a solution of ethyl (1-(4-((tetrahydro-2*H*-pyran-2-yl)oxy)phenyl)pent-4-yn-1-yl)glycinate (**16**, 28 mg, 0.082 mmol, 1 eq) and DMAP (2.0 mg, 16 µmol, 0.2 eq) in anhydrous DCM was added Et_3N (57.3 µL, 0.411 mmol, 5 eq). 2,2-dimethylchromane-6-sulfonyl chloride (64.3 mg, 0.247 mmol, 3 eq) was added at 0 °C and the mixture was warmed to rt and stirred for 5 days. The reaction mixture was concentrated with Celite and purified by silica gel column chromatography (10-15% EtOAc in *n*-pentane) to afford the product (35 mg, 0.061 mmol, 75%). ^{1}H NMR (400 MHz, $CDCl_3$) δ 7.69 – 7.60 (m, 2H), 7.06 – 6.99 (m, 2H), 6.95 – 6.90 (m, 2H), 6.85 (d, *J* = 8.9 Hz, 1H), 5.37 (t, *J* = 3.6 Hz, 1H), 4.98 (t, *J* = 7.5 Hz, 1H), 4.14 – 3.82 (m, 4H), 3.70 – 3.52 (m, 2H), 2.81 (ddd, *J* = 8.0, 6.5, 2.0 Hz, 2H), 2.22 – 1.98 (m, 4H), 1.95 (t, *J* = 2.6 Hz, 1H), 1.88 – 1.80 (m, 4H), 1.72 – 1.55 (m, 4H), 1.37 (s, 6H), 1.19 (td, *J* = 7.2, 0.8 Hz, 3H). ^{13}C NMR (101 MHz, $CDCl_3$) δ 170.23, 170.21, 158.09, 157.00, 156.95, 130.97, 130.05, 130.02, 129.81, 129.79, 129.54, 129.53, 127.58, 121.34, 117.88, 116.45, 116.39, 96.37, 96.29, 83.56, 75.77, 69.04,

62.21, 61.39, 59.19, 45.09, 45.03, 32.40, 30.82, 30.79, 30.41, 26.93, 25.27, 22.46, 18.86, 16.02, 14.14.

Ethyl *N*-((2,2-dimethylchroman-6-yl)sulfonyl)-*N*-(1-(4-hydroxyphenyl)pent-4-yn-1-yl)glycinate (18)

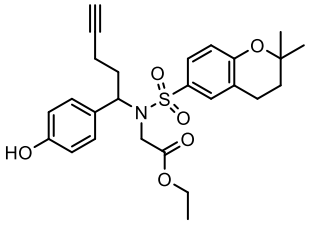

To a solution of ethyl *N*-((2,2-dimethylchroman-6-yl)sulfonyl)-*N*-(1-(4-((tetrahydro-2*H*-pyran-2-yl)oxy)phenyl)pent-4-yn-1-yl)glycinate (**17**, 13.5 mg, 24.0 μmol, 1 eq) in ethanol (0.47 mL, 0.05 M) was added TsOH (4.08 mg, 24.0 μmol, 1 eq). The mixture was stirred at rt for overnight. The reaction mixture was diluted in EtOAc and washed 1× with water and brine. The organic layer was dried over anhydrous Na_2SO_4, filtered and concentrated. The residue was purified by silica gel column chromatography (20-30% EtOAc in *n*-pentane) to obtain the product as a colorless oil (8.1 mg, 0.017 mmol, 70%). ^{1}H NMR (400 MHz, $CDCl_3$) δ 7.67 – 7.62 (m, 2H), 7.02 – 6.97 (m, 2H), 6.88 – 6.83 (m, 1H), 6.73 – 6.68 (m, 2H), 5.36 (s, 1H), 4.98 (t, *J* = 7.5 Hz, 1H), 4.13 – 3.99 (m, 2H), 3.99 – 3.60 (m, 2H), 2.80 (t, *J* = 6.7 Hz, 2H), 2.20 – 1.97 (m, 4H), 1.95 (t, *J* = 2.6 Hz, 1H), 1.84 (t, *J* = 6.8 Hz, 2H), 1.36 (s, 6H), 1.19 (t, *J* = 7.1 Hz, 3H). ^{13}C NMR (101 MHz, $CDCl_3$) δ 170.32, 158.15, 155.78, 130.86, 130.06, 129.83, 128.92, 127.59, 121.41, 117.91, 115.52, 83.46, 75.83, 69.14, 61.51, 59.16, 45.03, 32.40, 30.71, 26.93, 22.47, 16.00, 14.13.

2-(3-Methyl-3*H*-diazirin-3-yl)ethan-1-ol (19)

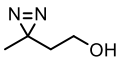

A round-bottom flask with 4-hydroxybutan-2-one (2.00 g, 22.7 mmol, 1 eq) under N_2 was cooled to 0 °C and 7 N NH_3 in MeOH (22.6 mL, 158 mmol, 7 eq) was added slowly. After 3 h, an anhydrous methanolic solution of NH_2OSO_3H (2.82 g, 25.0 mmol, 1.1 eq) was added dropwise at 0 °C. The resulting solution was allowed to warm to rt and stirred for overnight. The reaction mixture was evaporated to dryness in the reaction vessel under a stream of dry N_2 and the remaining residue was then resuspended in anhydrous MeOH and filtered. The filtrate was then concentrated under reduced pressure and re-dissolved in anhydrous MeOH (16 mL). The solution was cooled to 0 °C and Et_3N (4.84 mL, 34.7 mmol, 1.5 eq) was added. I_2 (2.36 g, 9.31 mmol, 0.4 eq) was then added in small portions until a dark brown color persisted in the solution for more than 10 min, indicating complete oxidation of the diaziridine intermediate. The solution was then diluted in EtOAc and the organic layer was washed with 1 M aq. HCl and sat. aq. $Na_2S_2O_3$. The organic layer was dried over anhydrous Na_2SO_4 and concentrated to obtain the product as a yellow liquid (0.20 g, 2.0 mmol, 21%). ^{1}H NMR (500 MHz, $CDCl_3$) δ 3.54 (t, *J* = 6.3 Hz, 2H), 2.02 (bs, 1H), 1.65 (t, *J* = 6.3 Hz, 2H), 1.08 (s, 3H). ^{13}C NMR (126 MHz, $CDCl_3$) δ 57.85, 37.07, 20.35.

2-(3-Methyl-3*H*-diazirin-3-yl)ethyl 4-methylbenzenesulfonate (20)

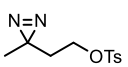

To a solution of 2-(3-methyl-3*H*-diazirin-3-yl)ethan-1-ol (**19**, 183 mg, 1.83 mmol, 1 eq) in pyridine (1.5 mL, 1.2 M) was added 4-methylbenzenesulfonyl chloride (523 mg, 2.74 mmol, 1.5 eq) at 0 °C and the mixture was stirred at rt for 1 h. The reaction

mixture was diluted in EtOAc and washed with 1 M aq. HCl, sat. aq. $NaHCO_3$, brine, and dried over anhydrous Na_2SO_4, filtered and concentrated. The residue was purified by silica gel column chromatography (10-15% EtOAc in *n*-pentane) to afford the product as a pale-yellow liquid (264 mg, 1.04 mmol, 57%). ^{1}H NMR (400 MHz, $CDCl_3$) δ 7.87 – 7.78 (m, 2H), 7.37 (d, *J* = 8.1 Hz, 2H), 3.96 (t, *J* = 6.4 Hz, 2H), 2.46 (s, 3H), 1.68 (t, *J* = 6.4 Hz, 2H), 1.01 (s, 3H). ^{13}C NMR (101 MHz, $CDCl_3$) δ 145.18, 132.85, 130.06, 128.13, 65.23, 34.31, 23.53, 21.82, 19.93.

Ethyl *N*-((2,2-dimethylchroman-6-yl)sulfonyl)-*N*-(1-(4-(2-(3-methyl-3*H*-diazirin-3-yl)ethoxy)phenyl)pent-4-yn-1-yl)glycinate (21)

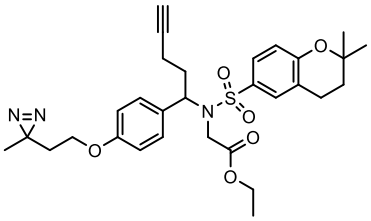

To a solution of ethyl *N*-((2,2-dimethylchroman-6-yl)sulfonyl)-*N*-(1-(4-hydroxyphenyl)pent-4-yn-1-yl)glycinate (**18**, 30 mg, 0.062 mmol, 1 eq) in anhydrous DMF (618 µL, 0.1 M) under N_2 was added Cs_2CO_3 (60.4 mg, 0.185 mmol, 3 eq). Subsequently, 2-(3-methyl-3*H*-diazirin-3-yl)ethyl 4-methylbenzenesulfonate (**20**, 23.6 mg, 93.0 µmol, 1.5 eq) was added and the reaction was stirred at rt for 5 h. The reaction mixture was diluted in EtOAc and washed with H_2O and brine, dried over anhydrous Na_2SO_4, filtered and concentrated. The residue was purified by silica gel column chromatography (10-15% EtOAc in *n*-pentane) to afford the product (8.7 mg, 0.015 mmol, 24%). ^{1}H NMR (500 MHz, $CDCl_3$) δ 7.67 – 7.61 (m, 2H), 7.07 – 7.01 (m, 2H), 6.87 – 6.82 (m, 1H), 6.79 – 6.74 (m, 2H), 4.99 (t, *J* = 7.5 Hz, 1H), 4.12 – 3.99 (m, 2H), 3.96 (d, *J* = 18.2 Hz, 1H), 3.82 (t, *J* = 6.2 Hz, 2H), 3.63 (d, *J* = 18.2 Hz, 1H), 2.80 (t, *J* = 6.7 Hz, 2H), 2.20 – 2.15 (m, 2H), 2.12 – 1.99 (m, 2H), 1.94 (t, *J* = 2.6 Hz, 1H), 1.84 (t, *J* = 6.8 Hz, 2H), 1.80 (t, *J* = 6.2 Hz, 2H), 1.37 (s, 6H), 1.19 (t, *J* = 7.2 Hz, 3H), 1.11 (s, 3H). ^{13}C NMR (126 MHz, $CDCl_3$) δ 170.18, 158.45, 158.12, 131.01, 130.06, 129.69, 129.41, 127.61, 121.37, 117.90, 114.59, 83.51, 75.79, 69.09, 63.02, 61.41, 59.20, 45.09, 34.39, 32.44, 30.82, 26.95, 24.37, 22.49, 20.38, 16.03, 14.16. LC-MS $[C_{30}H_{37}N_3O_6S+Na]^+$: 590.23 calculated, 590.07 found.

Reference

1. Baggelaar, M. P., Maccarrone, M. & van der Stelt, M. 2-Arachidonoylglycerol: A signaling lipid with manifold actions in the brain. *Prog. Lipid Res.* **71**, 1–17 (2018).
2. Mock, E. D., Gagestein, B. & van der Stelt, M. Anandamide and other *N*-acylethanolamines: A class of signaling lipids with therapeutic opportunities. *Prog. Lipid Res.* **89**, 101194 (2023).
3. Shrestha, N. *et al.* Peripheral modulation of the endocannabinoid system in metabolic disease. *Drug Discov. Today* **23**, 592–604 (2018).
4. Busquets-García, A., Bolaños, J. P. & Marsicano, G. Metabolic Messengers: endocannabinoids. *Nat. Metab.* **4**, 848–855 (2022).
5. Mechoulam, R. *et al.* Identification of an endogenous 2-monoglyceride, present in canine gut, that binds to cannabinoid receptors. *Biochem. Pharmacol.* **50**, 83–90 (1995).
6. Devane, W. A. *et al.* Isolation and structure of a brain constituent that binds to the cannabinoid receptor. *Science* **258**, 1946–1949 (1992).
7. Bisogno, T. *et al.* Cloning of the first sn1-DAG lipases points to the spatial and temporal regulation of endocannabinoid signaling in the brain. *J. Cell Biol.* **163**, 463–468 (2003).
8. Okamoto, Y., Morishita, J., Tsuboi, K., Tonai, T. & Ueda, N. Molecular Characterization of a Phospholipase D Generating Anandamide and Its Congeners. *J. Biol. Chem.* **279**, 5298–5305 (2004).
9. Blankman, J. L., Simon, G. M. & Cravatt, B. F. A Comprehensive Profile of Brain Enzymes that Hydrolyze the Endocannabinoid 2-Arachidonoylglycerol. *Chem. Biol.* **14**, 1347–1356 (2007).
10. Cravatt, B. F. *et al.* Molecular characterization of an enzyme that degrades neuromodulatory fatty-acid amides. *Nature* **384**, 83–87 (1996).
11. Liu, Y., Patricelli, M. P. & Cravatt, B. F. Activity-based protein profiling: The serine hydrolases. *Proc. Natl. Acad. Sci. U.S.A.* **96**, 14694–14699 (1999).
12. Patricelli, M. P., Giang, D. K., Stamp, L. M. & Burbaum, J. J. Direct visualization of serine hydrolase activities in complex proteomes using fluorescent active site-directed probes. *Proteomics* **1**, 1067–1071 (2001).
13. Baggelaar, M. P. *et al.* Development of an Activity-Based Probe and In Silico Design Reveal Highly Selective Inhibitors for Diacylglycerol Lipase-α in Brain. *Angew. Chem. Int. Ed.* **52**, 12081–5 (2013).
14. Baggelaar, M. P. *et al.* Highly Selective, Reversible Inhibitor Identified by Comparative Chemoproteomics Modulates Diacylglycerol Lipase Activity in Neurons. *J. Am. Chem. Soc.* **137**, 8851–8857 (2015).
15. Ogasawara, D. *et al.* Rapid and profound rewiring of brain lipid signaling networks by acute diacylglycerol lipase inhibition. *Proc. Natl. Acad. Sci. U.S.A.* **113**, 26–33 (2016).

16. Mock, E. D. *et al.* Discovery of a NAPE-PLD inhibitor that modulates emotional behavior in mice. *Nat. Chem. Biol.* **16**, 667–675 (2020).

17. Cisar, J. S. *et al.* Identification of ABX-1431, a Selective Inhibitor of Monoacylglycerol Lipase and Clinical Candidate for Treatment of Neurological Disorders. *J. Med. Chem.* **61**, 9062–9084 (2018).

18. Johnson, D. S. *et al.* Discovery of PF-04457845: A highly potent, orally bioavailable, and selective urea FAAH inhibitor. *ACS Med. Chem. Lett.* **2**, 91–96 (2011).

19. Müller-Vahl, K. R. *et al.* Monoacylglycerol Lipase Inhibition in Tourette Syndrome: A 12-Week, Randomized, Controlled Study. *Mov. Disord.* **36**, 2413–2418 (2021).

20. D'Souza, D. C. *et al.* Efficacy and safety of a fatty acid amide hydrolase inhibitor (PF-04457845) in the treatment of cannabis withdrawal and dependence in men: a double-blind, placebo-controlled, parallel group, phase 2a single-site randomised controlled trial. *Lancet Psychiatry* **6**, 35–45 (2019).

21. Hsu, K.-L. *et al.* DAGLβ inhibition perturbs a lipid network involved in macrophage inflammatory responses. *Nat. Chem. Biol.* **8**, 999–1007 (2012).

22. Khasabova, I. A. *et al.* Inhibition of DAGLβ as a therapeutic target for pain in sickle cell disease. *Haematologica* **108**, 859–869 (2023).

23. Jenniches, I. *et al.* Anxiety, Stress, and Fear Response in Mice with Reduced Endocannabinoid Levels. *Biol. Psychiatry* **79**, 858–868 (2016).

24. Cavener, V. S. *et al.* Inhibition of Diacylglycerol Lipase Impairs Fear Extinction in Mice. *Front. Neurosci.* **12**, 1–10 (2018).

25. Janssen, F. J. *et al.* Discovery of Glycine Sulfonamides as Dual Inhibitors of *sn*-1-Diacylglycerol Lipase α and α/β-Hydrolase Domain 6. *J. Med. Chem.* **57**, 6610–6622 (2014).

26. Dong, A. *et al.* A fluorescent sensor for spatiotemporally resolved imaging of endocannabinoid dynamics in vivo. *Nat. Biotechnol.* (2021) doi:10.1038/s41587-021-01074-4.

27. Cooke, M. & Kazanietz, M. G. Overarching roles of diacylglycerol signaling in cancer development and antitumor immunity. *Sci. Signal.* **15**, 1–27 (2022).

28. Helfand, B. T., Mendez, M. G., Pugh, J., Delsert, C. & Goldman, R. D. Diacylglycerol-dependent Binding Recruits PKCθ and RasGRP1 C1 Domains to Specific Subcellular Localizations in Living T Lymphocytes. *Mol. Biol. Cell.* **15**, 2932–2942 (2004).

29. Katti, S. S. *et al.* Structural anatomy of Protein Kinase C C1 domain interactions with diacylglycerol and other agonists. *Nat. Commun.* **13**, 1–11 (2022).

30. Griner, E. M. & Kazanietz, M. G. Protein kinase C and other diacylglycerol effectors in cancer. *Nat. Rev. Cancer* **7**, 281–294 (2007).

31. Pan, Q. *et al.* Protein kinase Cε is a predictive biomarker of aggressive breast cancer and a validated target for RNA interference anticancer therapy. *Cancer Res.* **65**, 8366–8371 (2005).

32. Bae, K. M. *et al.* Protein kinase Cε is overexpressed in primary human non-small cell lung cancers and functionally required for proliferation of non-small cell lung cancer cells in a p21/Cip1-dependent manner. *Cancer Res.* **67**, 6053–6063 (2007).

33. Aziz, M. H. *et al.* Protein kinase Cε interacts with signal transducers and activators of transcription 3 (Stat3), phosphorylates Stat3Ser727, and regulates its constitutive activation in prostate cancer. *Cancer Res.* **67**, 8828–8838 (2007).

34. Huang, B. *et al.* The expression and role of protein kinase C (PKC) epsilon in clear cell renal cell carcinoma. *J. Exp. Clin. Cancer Res.* **30**, 1–9 (2011).

35. Lau, E. *et al.* PKCε promotes oncogenic functions of ATF2 in the nucleus while blocking its apoptotic function at mitochondria. *Cell* **148**, 543–555 (2012).

36. Porter, S. N. & Magee, J. A. PRKCH regulates hematopoietic stem cell function and predicts poor prognosis in acute myeloid leukemia. *Exp. Hematol.* **53**, 43–47 (2017).

37. Kim, W. K. *et al.* Sustained mutant KIT activation in the Golgi complex is mediated by PKC-θ in gastrointestinal stromal tumors. *Clin. Cancer Res.* **23**, 845–856 (2017).

38. Hill, K. S. *et al.* Protein kinase Cα suppresses Kras-mediated lung tumor formation through activation of a p38 MAPK-TGFβ signaling axis. *Oncogene* **33**, 2134–2144 (2014).

39. Chen, S., Wang, Y., Zhang, Y. & Wan, Y. Low expression of PKCα and high expression of KRAS predict poor prognosis in patients with colorectal cancer. *Oncol. Lett.* **12**, 1655–1660 (2016).

40. Oster, H. & Leitges, M. Protein kinase C α but not PKCζ suppresses intestinal tumor formation in $Apc^{Min/+}$ mice. *Cancer Res.* **66**, 6955–6963 (2006).

41. Hsu, A. H. *et al.* Crosstalk between PKCα and PI3K/AKT Signaling Is Tumor Suppressive in the Endometrium. *Cell Rep.* **24**, 655–669 (2018).

42. Dowling, C. M. *et al.* Protein kinase C beta II suppresses colorectal cancer by regulating IGF-1 mediated cell survival. *Oncotarget* **7**, 20919–20933 (2016).

43. D'Costa, A. M. *et al.* The proapoptotic tumor suppressor protein kinase C-δ is lost in human squamous cell carcinomas. *Oncogene* **25**, 378–386 (2006).

44. Baryła, M. *et al.* Oncometabolites—A Link between Cancer Cells and Tumor Microenvironment. *Biology* **11**, 1–18 (2022).

45. Zhong, X. P. *et al.* Enhanced T cell responses due to diacylglycerol kinase ζ deficiency. *Nat. Immunol.* **4**, 882–890 (2003).

46. Olenchock, B. A. *et al.* Disruption of diacylglycerol metabolism impairs the induction of T cell anergy. *Nat. Immunol.* **7**, 1174–1181 (2006).

47. Salerno, F., Paolini, N. A., Stark, R., Von Lindern, M. & Wolkers, M. C. Distinct PKC-mediated posttranscriptional events set cytokine production kinetics in $CD8^+$ T cells. *Proc. Natl. Acad. Sci. U.S.A* **114**, 9677–9682 (2017).

48. Stinchcombe, J. C. *et al.* Ectocytosis renders T cell receptor signaling self-limiting at the immune synapse. *Science* **380**, 818–823 (2023).

49. Arranz-Nicolas, J. *et al.* Diacylglycerol kinase ζ limits IL-2-dependent control of PD-1 expression in tumor-infiltrating T lymphocytes. *J. Immunother. Cancer* **8**, 1–13 (2020).

50. Shin, M., Buckner, A., Prince, J., Bullock, T. N. J. & Hsu, K. L. Diacylglycerol Lipase-β Is Required for TNF-α Response but Not $CD8^+$ T Cell Priming Capacity of Dendritic Cells. *Cell Chem. Biol.* **26**, 1036-1041 (2019).